Paper accepted for presentation at 2009 IEEE Bucharest Power Tech Conference, June 28th - July 2nd, Bucharest, Romania

Wind Turbine Modelling for Transient Analysis: Application to the Spanish Grid Code

A. J. Pujante-López, J. A. Fuentes-Moreno, E. Gómez-Lázaro, A. Molina-García and M. Cañas-Carretón

***Abstract*—The aim of this paper is the implementation of a dynamic model of a DFIG variable speed wind turbine where all the parameters are known and that can be used for different types of dynamic studies as, for example, the evaluation of its transient state and steady state response, using different control strategies, when it is submitted to any type of fault, and in this type of events are studied the compliance degree of the imposed requirements by the Spanish Grid Code. Another application of the above DFIG model is that it can also be used as a building block for creating an aggregated model of a wind farm and, thus, studying the behaviour of the whole wind farm under such faults.**

***Index Terms*—Wind Turbine, DFIG modelling, voltage dips, grid codes, power control.**

I. Introduction

Voltage dips are short duration reductions in rms voltage (between 10% and 90%) of the voltage at a point in the electrical system, which lasts for half a cycle to 1 min, [1]. The duration of voltage dips is described as the total time interval between the point on wave of sag initiation and recovery, [2]. They are caused by faults in the electric supply system and the starting of large loads, such as motors. Voltage dips are generally considered a power quality problem of equal importance as long and short interruptions in the supply. The interests in voltage dips are increasing because they cause the detrimental effects on several sensitive equipments such as adjustable-speed drives, process-control equipments, and computers. Such equipments can be tripped when the voltage drops below 90% of the rated voltage for longer than a few cycles, [3], [4]. In accordance with the practice in wind farms, wind turbines are disconnected from the grid when the terminal voltage fell below 80-90%, [5], [6]. Even relays and contactors in motor starters can be sensitive to voltage dips, resulting in shutdown of a process when they drop out, [7].

Voltage dips are mainly due to short-circuits and earth faults in the grid, [8]. These faults in the power system, even far away from the location of the wind farm, or any other power installation, can generate a voltage dip at the connection point of the wind turbines. Factors governing the magnitude and duration of voltage dips include the fault impedance and location, the configuration of the power network, and the system protective relay design and operation, [7]. This last aspect is important since voltage dip condition lasts until the fault is cleared by a protective device. Solutions to the voltage dip effects must be implemented in the customer facility, since although it is possible for the utility to reduce the number of faults through design practices and specific equipment, it is impossible to avoid faults on the power system, [7]. Therefore, in wind farms, the solution must be installed at the wind farm interconnection point with the electrical grid or at the wind turbine level.

The installed capacity of wind power generation has grown very fast in the past years, increasing dramatically the level of wind power generation into existing utilities' network. On the other hand, the rating of large wind farms reaches rating of conventional generating units and this development has carried out to requirements of how to connect wind farms to the grid. Until now, these grid codes —specified by the transmission system operators— mainly dealed with how a wind farm should operate in steady state while requirements recently imposed in some countries dealed with how a wind installation response to grid faults must be addressed, [9]. These are commonly referred to as the fault ride-through specifications. Specifically, national grid codes are requiring uninterrupted generation throughout power system disturbances supporting the network voltage and frequency, and therefore, extending characteristics such as low voltage ride through, or reactive and active power capabilities, [9], [10].

II. Spanish Grid Code

In Spanish case, REE —the transmission system operator Red Eléctrica de España— grid code, specifies that the wind farm must support voltage dips, at the point of interconnection with the transmission network, without tripping. The voltage-time curve that limits the magnitude and duration of the voltage dips, produced by single-phase-to-ground, two-phase-to-ground and three-phase short-circuits, is shown in figure 1. For non-earthed two-phase short-circuits, the voltage limit is chosen at 0.6 p.u. instead of 0.2 p.u.

A. Balanced three-phase faults

Wind farms will not absorb reactive power during either balanced three-phase faults, or the voltage recovery period after the clearance of the fault, Nonetheless, reactive power

The authors would like to thank "Ministerio de Educación y Ciencia" –ENE2006-15422-C02-01/ALT and ENE2006-15422-C02-02/ALT– and "Junta de Comunidades de Castilla-La Mancha" –PAI08-0145-9976– for the financial support.

Emilio Gómez, Miguel Cañas and Antonio Jesús Pujante are with Renewable Energy Research Institute, Universidad de Castilla-La Mancha, Albacete 02071 Spain. (e-mails: emilio.gomez@uclm.es, antoniojesus.pujante@uclm.es, miguel.canas@uclm.es). (phone: +34 967 599 200, fax: +34 967 555 321)

Juan Álvaro Fuentes and Ángel Molina are with the Department of Electrical Engineering, Universidad Politécnica de Cartagena, Cartagena 30202 Spain; (emails: juanalvaro.fuentes@upct.es, angel.molina@upct.es). (phones: +34 968 325 604, +34 968 325 462, fax: +34 968 325 356)

978-1-4244-2235-7/09/$25.00 ©2009 IEEE

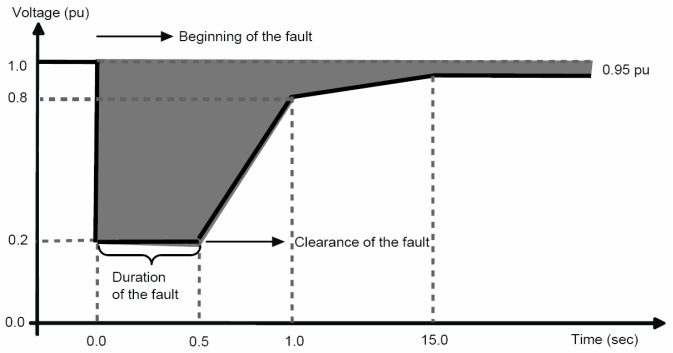

Fig. 1. Voltage-time curve that the generation facility must support

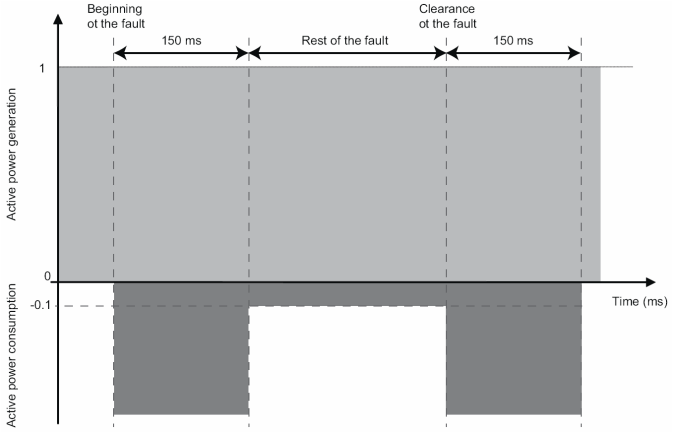

Fig. 2. Grid Code requirements for active power (balanced 3-phase faults)

absorptions may occur during a period of 150 ms after the beginning of the fault, and also 150 ms after the clearance of the fault, although the following requirements must be met:

- The net reactive power consumption of the wind farm during the 150 ms interval after the beginning of the fault, in 20 ms cycles, must not exceed 60% of its rated power.
- The net reactive energy consumption of the wind farm after the clearance of the fault must not exceed 60% of its rated power, and the reactive current, in 20 ms cycles, must not exceed 1.5 times the rated current.

In terms of active power, the wind farm at the grid connection point must not absorb active power during the fault or the voltage recovery period after the clearance of the fault. On the other hand, absorption of active power is accepted for 150 ms after the beginning of the fault and further 150 ms after the clearance of the fault, figure 2. During the rest of the fault, the active power consumptions are additionally may take place up to a 10% of the wind farm rated power.

Regarding currents, wind farm must provide the maximum generation of reactive current to the electrical network at the grid connection point during the fault and later in the voltage recovery period. In any case, this current must be located in the shaded area in figure 3, within 150 ms after the beginning of the fault or after the clearance of the fault. Therefore, the wind farm must generate reactive current with voltages below 0.85 pu, and it must not consume reactive power between 0.85 pu and the minimum admissible voltage for average operation of the electrical network.

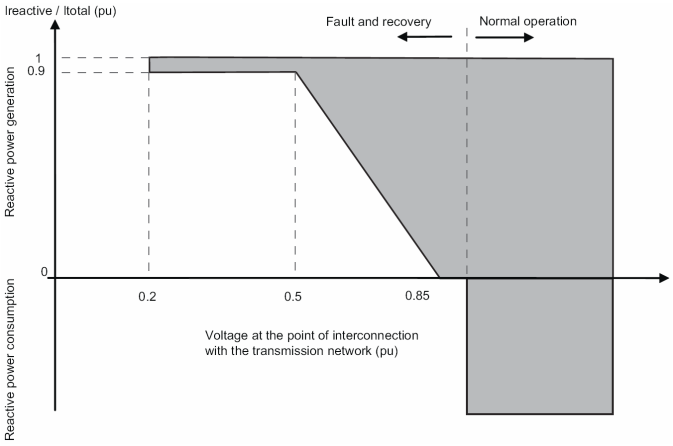

Fig. 3. Grid Code requirements for current and reactive power (balanced 3-phase faults)

B. Unbalanced two-phase and single-phase faults

During unbalanced two-phase and single-phase faults, as well as in the voltage recovery period after the clearance of the fault, wind farms must not absorb reactive power at the grid connection point.

Nonetheless, reactive power absorptions are admitted during a period of 150 ms after the beginning of the fault and a period of 150 ms after the clearance of the fault, with two constraints:

- The net reactive power consumption of the wind farm, during the 150 ms interval after the beginning of the fault, will not exceed the 40% of its rated power during a period of 100 ms.
- The net reactive power consumption of the wind farm after the fault clearance, in 20 ms cycles, will not exceed the 40% of its rated power.

Additionally, transitory consumption is allowed during the rest of the fault with two constraints:

- The net active consumption must not exceed the 45% of the equivalent rated active energy of the installation during a period of 100 ms.
- The consumption of active power, in cycles of 20 ms, must not exceed the 30% of its rated active power.

III. Voltage dip characterization

Voltage-dip characterization concerns the quantification of voltage-dip events through a limited number of parameters, [11]. Most methods for voltage dip characterization use two parameters to quantify the severity of a voltage dip — magnitude (or "remaining voltage") and duration—, [3], [12]–[14]. However, voltage dips can be far more complicated than this type of characterization can show:

- Usually, methods are based on the lowest remaining voltage and the longest duration of all the three voltages. This causes some problems, but it is an appropriate

approximation for balanced dips, whereas the majority of dips are unbalanced, [13].
- Dip depth and phase-angle jump information can be required along with start and end times, [12].
- Therefore, some authors are researching other methods to characterize unbalanced dips, being based on measurements or applying the basic circuit theory in the faults, [11].
- It is usually assumed that the voltage profile during voltage dip is rectangular, failing in the characterization of non-rectangular dip, overestimating it, [3], [11]. This can be important to many industrial customers with large induction motor loads or in the case of wind farms.
- This methodology is not adequate to multistage voltage dips events, in which the fault can evolve to a different type.

Basically, the input data to the characterization methods can be fitted in:

- Monitoring the lowest remaining voltage and the longest duration of all the three voltages.
- Monitoring all the voltages waveforms with an adequate sample rate.
- Monitoring of $\sqrt{V_d^2 + V_q^2}$ in a vector controller, using a phase-locked loop —PLL–, [4].

Two methods to obtain three-phase voltage dip characterization —'ABC classification' and 'symmetrical components classification'— were exposed and compared in [12]. It is concluded that ABC classification —due to its simplicity— is more used than the symmetrical components.

In [15], theoretical relations between the minimum phase-to-neutral voltage —V_{PN}— and the minimum phase-to-phase voltage —V_{PP}— are presented for the seven types of dips, defined in [12]:

- Type A: all phases experience the same retained voltage and phase-angle jump.

$$V_{PP} = V_{PN} \tag{1}$$

- Type B: It is not common because it is seen only when a line to ground fault occurs at the same voltage level or at a location connected by star-star transformer grounded at both sides.

$$V_{PP} = \frac{\sqrt{\left(\frac{1}{2} + V_{PN}\right)^2 + \frac{3}{4}}}{\sqrt{3}} \tag{2}$$

- Type C: It is a reduction of the voltage in two phases. It is caused by a line to line fault or by a propagation of dip type B through a delta-star connected transformer.

$$V_{PP}^2 = \frac{4}{3}V_{PN}^2 - \frac{1}{3} \tag{3}$$

- Type D: It is caused by a propagation of a type C dip through a delta-star windings connected transformer. It is a voltage drop in one phase.

$$V_{PP}^2 = \frac{1}{4} + \frac{3}{4}V_{PN}^2 \tag{4}$$

- Type E: It shows a symmetrical relation between PP and PN voltage like type A. This dip is rare as type B by the same reasons.
- Type F: It is a reduction of the voltage in one phase, caused by the propagation of a line to line to ground fault through a delta-star connected transformer.

$$3V_{PP}^2 = (2 + \frac{1}{3})V_{PN}^2 + \frac{1}{3}V_{PN} + \frac{1}{3} \tag{5}$$

- Type G: These dips are obtained from the propagation of a dip type F through a delta-star connected transformer.

$$V_{PP} = -0.0707 + \frac{\sqrt{3.112 \cdot V_{PN}^2 - 0.327}}{1.556} \tag{6}$$

In this classification, voltage dip types D and F —C and G—, are similar, making difficult their distinction from the measurements without knowing the fault types that caused them, [16].

IV. Wind Turbine Modelling and Implementation

The DFIG wind turbine is a 2 MW, 2 pole pairs and 50 Hz frequency. The most important parameters are in Table I, this model was previously built and simulated in [17]. The mechanical and the electrical model of this wind turbine are also included in [17]. As explained in such paper the optimum speed vs power curve is used as a reference in the active power control of electrical converter.

TABLE I
Parameters of wind turbine and induction machine

Parameter (unit)	Value
Rated Power (MVA)	2.00
Rated Voltage (kV)	0.69
Rated Current (kA)	2.00
Rated Frequency (Hz)	50
Stator/Rotor turns ratio	0.38
Pole numbers	4
Stator Resistance (pu)	0.34
Rotor Resistance (pu)	0.009
Stator leakage Inductance (pu)	0.105
Rotor leakage Inductance (pu)	0.111
Magnetizing Inductance (pu)	3.34
Magnetizing Resistance (pu)	47.61
Angular Moment of Inertia (s)	3.82
Mechanical Damping (pu)	0.01
Turbine rotor speed range (rpm)	9-19
Rated rotor speed (rpm)	1500
Rated wind speed (m/s)	13
Rotor diameter (m)	80
Gearbox ratio	1:100

The WT model has been implemented using a commercial simulation software PSCAD. This software package offers suitable models for evaluating DFIG wind turbine [18]. Moreover, it includes a generic wind turbine governor and different wind resource patterns, as well as it has the capability to generate differents three-phase faults into the grid connection point. The main block diagram developed in PSCAD is shown in Figure 4. This model includes a DFIG shaft (high speed) connected to the wind turbine shaft (low speed) by means of an ideal gearbox between them.

The stator terminals are directly connected to the grid, and the rotor terminals are indirectly connected to the grid by means of a back-to-back power converter.

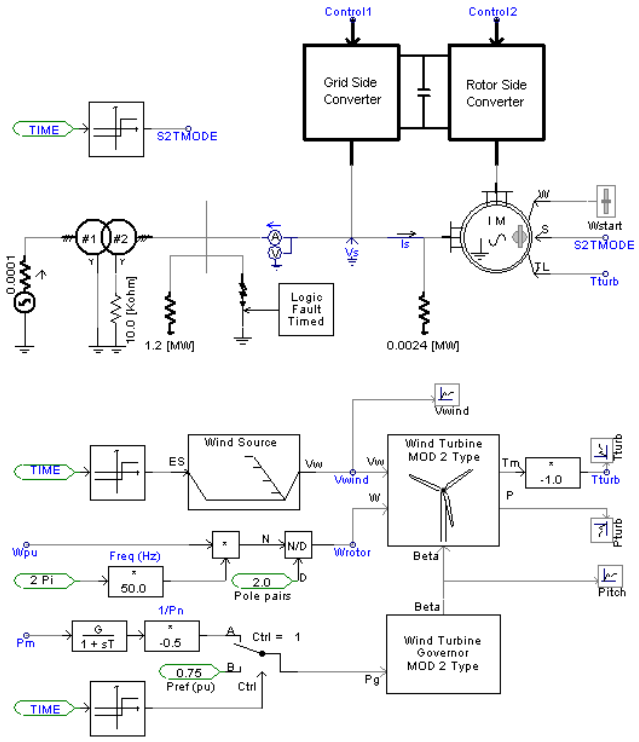

Fig. 4. Main block diagram containing DFIG, Wind Turbine and power converters.

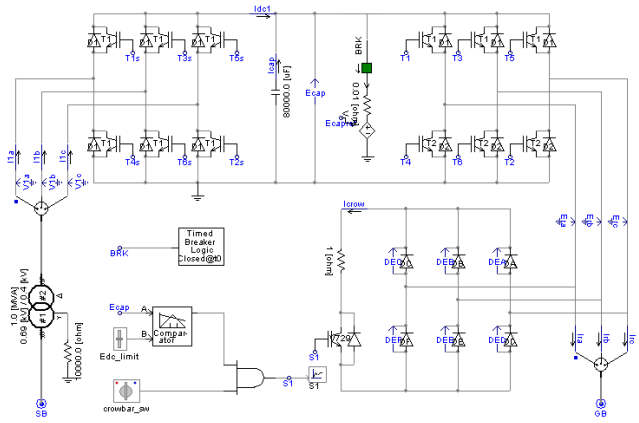

Fig. 5. Back-to-back connected power converter bridges and crowbar protection circuit.

A. The power converter controls

The wind turbine governor has the task of setting the pitch angle β, in order to limit the mechanical power for the wind turbine. The block diagram for the control of DFIG model is mainly based on the general control structure presented in [19]. The Rotor Side Converter (RSC) controls the stator active and reactive powers, whereas the Grid Side Converter (GSC) holds constant the DC link voltage. For simulating purposes, the control schemes for both converters, which includes the crowbar protection circuit and their respective control functions, are shown in Figure 5.

Two different PWM strategies are implemented to control the converters: a Carrier Triangular technique is used for the GSC; whereas, for theRSC, a Hysteresis Band technique is applied. The electrical grid model includes a grid transformer and a voltage source, which details can be consulted in [17].

The RSC control includes two typical PI controller with output saturated. The first one controls the stator active power and the other one controls reactive power (P_s, Q_s) throught the rotor currents into dq reference frame as show in [17].

The GSC control includes three typical PI controller with output saturated. The first one controls the DC link voltage, whereas the other ones control the stator currents into the dq reference frame (I_{sd} and I_{sq}) through a decoupled control scheme as presented in [17]. The parameters for the five PI controllers are included in table II.

TABLE II
CONTROL PARAMETERS AND SATURATION CONSTANTS

Active power control (Ps)		Reactive power control(Qs)	
Parameter	Value	Parameter	Value
Kp1	0.001	Kp2	0.05
Ki1	0.002	Ki2	2.0
Irqmax	+100	Irdmax	+100
Irqmin	-10	Irdmin	-10
DC-link voltage control (Edc)		Current stator controls (Isd, Isq)	
Parameter	Value	Parameter	Value
Kp3	20.0	Kp4	10.0
Ki3	100	Ki4	100
Isdmax	+2.0	Vsmax	+15.0
Isdmin	-2.0	Vsmin	-15.0

The PI parameters are optimized during the three-phase faults by means of an optimum run block, since this block is suitable for the optimization of several real variables using a proper Objective Function (OF). In this paper the OF selected is corresponding with the linear combination of the errors in active and reactive stator powers, whereas the variables to optimize are chosen as the PI parameters of the active and reactive stator power PI regulators shown in table II.

V. RESULTS

In this section, several simulations of the electrical system with the implemented wind turbine model in PSCAD software are presented. In this way, Figures 7, 8 and 9 show the global results, moreover the Figures 10, 11 and 12 include the zoom of the most important results. In all cases, the (a) simulation represents the WT response under a single-phase to ground voltage sag —blue trace—, the (b) and (c) simulations represent the WT behaviour under two-phase voltage sags, ground —green trace— and non ground —red trace— referenced, respectively; while the (d) and (e) simulations correspond to the WT responses under three-phase voltage sags, ground —cyan trace— and non ground —magenta trace— referenced, respectively. On the other hand, the wind turbine always starts with speed control mode until $t = 0.5s$, being the rotor speed reference 0.9 pu and the wind speed is keeping constant at $13.5m/s$ during all simulations. After that, it is assumed that the IG is started-up, and the IG torque control mode set-up. Although the wind turbine pitch control is enabled to limit the generated mechanical power, the β angle is kept zero for whole

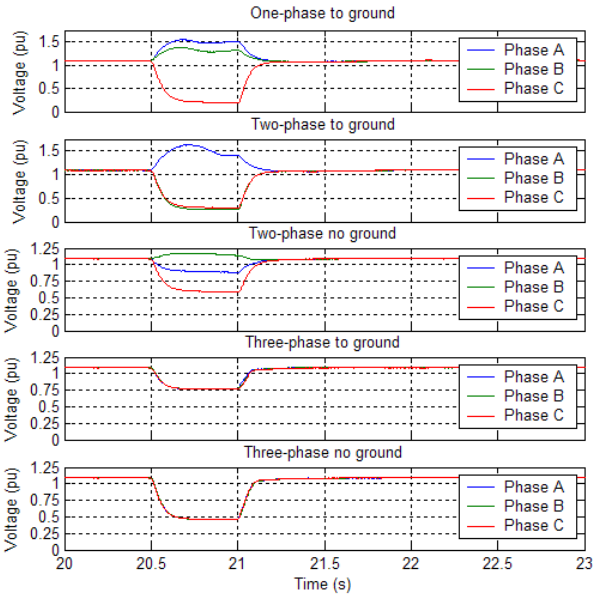

Fig. 6. Three-phase different faults: unbalanced and balanced voltage sags

simulations, due mainly to the lack of wind speed fluctuations. For this reason the system reaches the steady state around $t = 15s$ before the voltage dip occurs at time $t = 20.5s$, the system reaches the steady state again at the end of simulation time $t = 30s$.

The figure 6 shows five different three-phase faults as examples of voltage sags used into the simulation. The three first plots are unbalanced single-phase and two-phase faults, respectively, whereas the two last plots are balanced three-phase faults. Only the third and the fifth plots are voltage sags non ground referenced.

Concerning the electrical simulation results, Figure 7 shows the voltage and current evolutions and Figure 8 presents the active and reactive power values. Then, the three first plots in Figure 7 include the stator and rotor voltages, and the dc-link voltage, whereas the other ones include the generator, stator and rotor currents of the DFIG, respectively. First plot illustrates that the three-phase stator voltages are slightly higher than 1 pu, both before and after the voltage sag, but all of the voltage dips have at least one of the A, B or C phase under 0.8 pu for a period of $0.5s$, being the recovery time $t = 0.25s$ after the voltage sag is cleaned, as can be shown in figure 6. It must be noted that in unbalanced faults, i.e. one or two phases are affected, but the other phase or phases try to compensate the suddenly voltage drop, for this reason the three-phase voltage computation can be less deep than the three voltages, as can be seen when the first plot in figure 10 is compared with the plots corresponding in figure 6. Nevertheless, the voltage sags generator has configured the same fault resistances (R_{ON} and R_{OFF}) values in every cases. Specially, in (a) and (b) cases the voltage sags drop to 0.25 pu in one and two phases, respectively, but the other phases rise up close to 1.5 pu. In (c) case the voltage sag drops to 0.6 pu in one phase and 0.9 pu in the other phase, but the third phase rises to 1.2 pu. In (d) and (e) cases the three-phase voltage

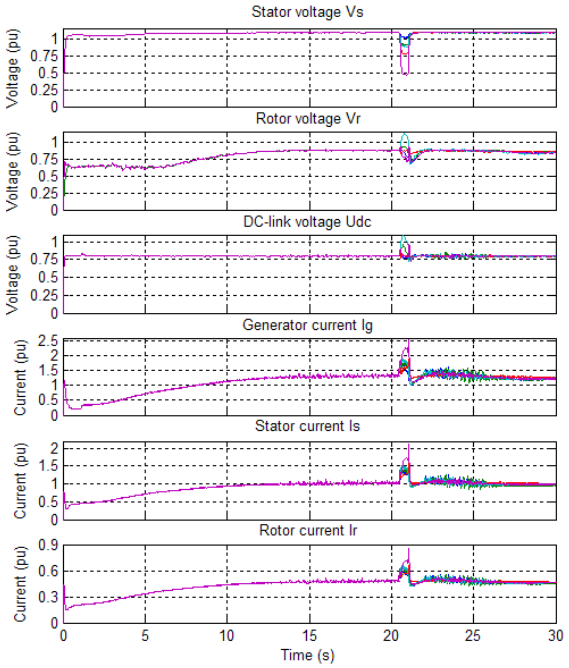

Fig. 7. Total simulation results. Voltages and currents

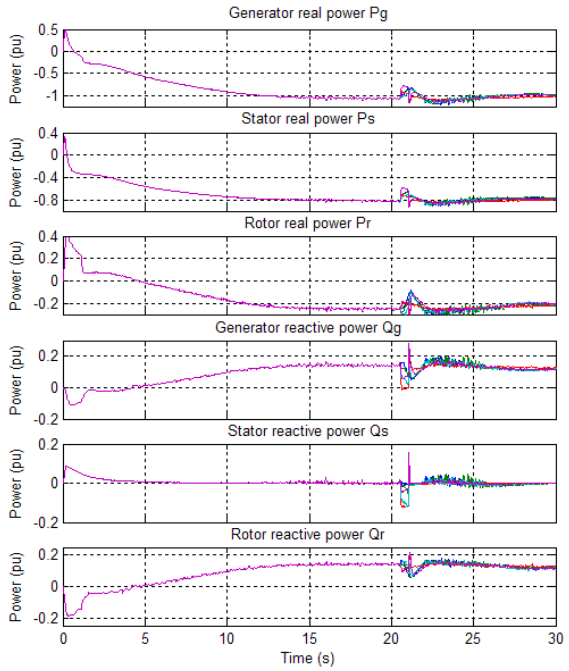

Fig. 8. Total simulation results. Power variables

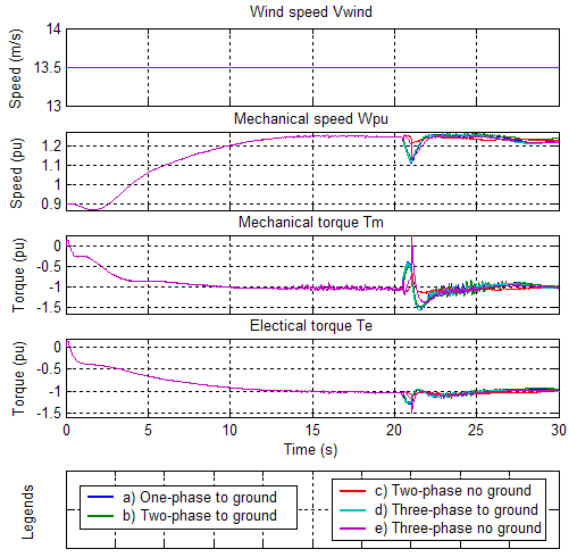

Fig. 9. Total simulation results. Mechanical variables

sags drop to 0.75 and 0.5 pu, respectively.

The next plot shows that the three-phase rotor voltages are greater than 0.85 pu in steady state, after the time $t = 10s$. When the voltage sag occurs at $t = 20.5s$ (Fig. 10), the rotor voltage drop to 0.7 pu in (a) and (d) cases, being around 0.8 pu in (e) case; whereas in (b) and (d) cases this voltage rises up 0.95 and 1.1 pu, respectively. The rotor voltages reach the steady state in $t = 22s$. The third plot illustrates that the dc-link voltages are around 0.8 pu in steady state, after the initial period, but at $t = 20.5s$ (Fig. 10) this dc-link voltage changes from 1.1 to 0.75 pu in the worst (d) case, being less the variation in (b) and (e) cases, since these voltages vary from 0.95 to 0.75 pu. The (a) and (b) cases do not change slightly. The dc-link voltages do not reach the steady state until $t = 21.5s$.

Next plot shows that the three-phase generator currents reach the steady state at $t = 15s$, being the rated value around 1.3 pu, because the base current was selected as the rated stator current. When the voltage dip appears (Fig. 10) these currents rise up 1.5 pu in (c) case and 2.3 pu in (e) case until $t = 21s$, being the other cases between these limits, respectively. Then the (c) and (d) current curves vary suddenly to 1.9 and 2.5 pu, while the other current curves fall close to 1 pu in a short transient period, and all the currents reach the next steady state around $t = 22s$, with a small variation into their rate values, but in $t = 27s$ these currents variations are compensated. It must be taken into account that the maximum allowed current during the voltage sag is 1.5 times of the rated current value. In the generator current this maximum value is corresponding with 1.95 pu. The last two plots illustrate the same current evolutions but in stator and rotor currents. In these cases the stator and rotor currents reach also the steady state at $t = 15s$, being their rated values 1 and 0.5 pu, respectively.

Regarding to the active and reactive power curves, Figure 8 presents the active power values in the three first plots, whereas the other ones include the reactive power values of the

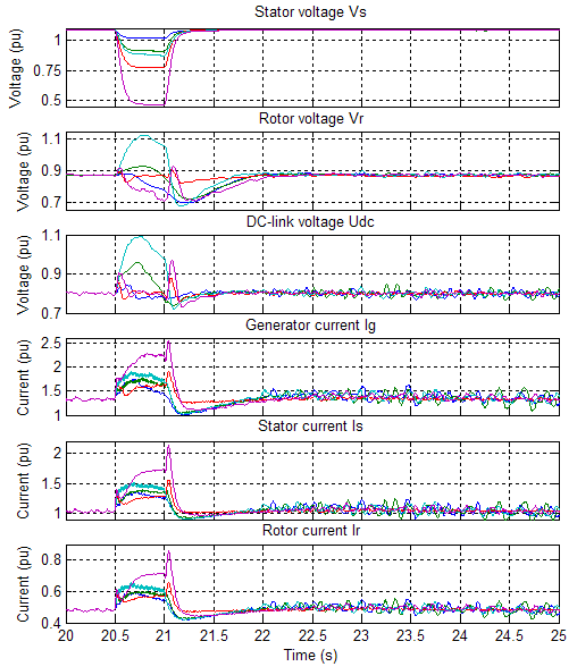

Fig. 10. Zoom simulation results. Voltages and currents

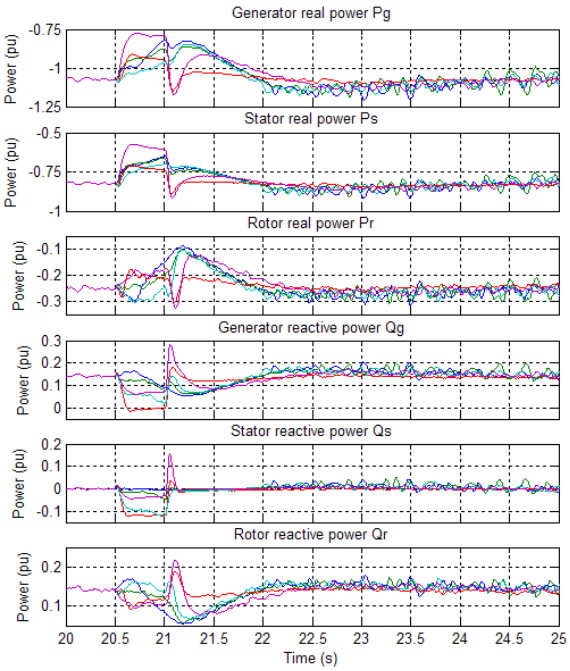

Fig. 11. Zoom simulation results. Power variables

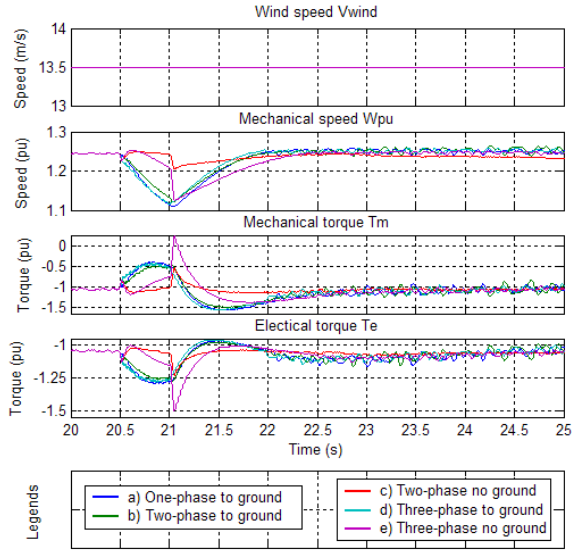

Fig. 12. Zoom simulation results. Mechanical variables

DFIG. In all cases, the generator power is considered as the combination of stator and rotor powers —see first plot—. From these results, stator and rotor active power curves are presented into second and third plots, being these results quite similar. Second plot shows that all the active powers are greater than zero (0.5 pu) in the initial period. Because, at the beginning, the DFIG works as motor, and from $t = 0.5s$, the stator active powers are less than zero, and the DFIG operates as generator, but in sub-synchronous mode until $t = 5s$, because the rotor active powers are greater or equal to zero (0.4 pu). From $t = 5s$ these rotor powers are also negative and DFIG changes to super-synchronous mode until the end. As shown the stator and rotor powers reach the steady state around $t = 15s$, being the rated values -0.8 and -0.25 pu, respectively. When the voltage sag occurs (Fig. 11) these stator powers fall close to -0.73 pu in (a)-(d) cases and -0.4 pu in (e) case, respectively until $t = 21s$, then these powers are recovered in $t = 22s$, while the rotor power curves vary between -0.1 and -0.3 pu during the voltage dip, and the steady states are reached in $t = 22.5s$. In all power curves appear a short transient period with a low variation into their rated values until $t = 27s$, after the voltage sag is cleaned. It must be taken into account that active power consumption during the voltage sag and in the voltage recovery period after the clearance of the fault is not allowed. In the generator active powers the minimum values are -0.75 pu, i.e. during the voltage sag the WT keeps on working as generator.

Next plots are the reactive power curves, being the generator power as the combination of stator and rotor powers —see forth plot—. From these results, stator and rotor reactive power curves are included into fifth and sixth plots, being these evolutions quite similar. Fifth plot shows that all the reactive powers are positive (0.09 pu) until $t = 5s$, then the stator powers are keeping to zero in the steady state; whereas the rotor powers are negative (-0.2 pu) until $t = 5s$, but they reach the steady state in $t = 13s$ with a positive value around 0.16 pu. At $t = 20.5s$ (Fig. 11) these stator powers fall close to -0.12 pu in (c)-(d) cases and -0.04 pu in (b) and (e) cases, while (a) case is keeping to zero, respectively until $t = 21s$, then these powers are recovered in $t = 21.2s$, but (c) and (e) cases the stator power rise up 0.03 and 0.16 pu, respectively; while the rotor power curves vary between 0.05 and 0.22 pu during the voltage dip, and the steady states are reached in $t = 22.5s$. In all power curves appear a short transient period with a low variation into their rated values until $t = 27s$, after the voltage sag is cleaned. It must be taken into account that the maximum allowed reactive power consumption during the voltage sag is 0.6 and 0.4 times the rated reactive power value in the balanced and unbalanced faults, respectively; assuming this rated value as 0.2 pu in the generator reactive power, then the maximum values are corresponding with 0.12 and 0.08 pu, respectively. In (a) and (b) cases the generator reactive power are 0.16 and 0.12 pu, respectively, being these powers less than 0.07 pu in (d) and (e) cases, even the reactive power is 0.0 pu in (c) case.

Regarding the mechanical simulation results, Figure 9 shows three mechanical plots and one electrical plot. In first plot —wind speed—, it can be seen that the wind speed do not vary of 13.5 in all cases. Second plot illustrates the rotor mechanical speed curves, which changes from 0.9 to 0.8 pu, in the initial period, and the DFIG is operating in sub-synchronous mode until $t = 5s$, since the rotor speed is lower than 1.05 pu. After that the DFIG is operating in super-synchronous mode from $t = 5s$, since the slip is also above 0.05 pu. The steady state is reached at $t = 15s$ in all cases with a rated value around 1.25 pu. When voltage dip occurs (Fig. 12) the rotor speeds change. For example in (a), (b) and (d) curves the speed drops from 1.25 to 1.12 pu at $t = 21s$, whereas (c) and (e) curves the speed drops slowly to 1.2 pu at $t = 21s$, then only the e) curve falls suddenly to 1.13 pu and all curves rise to their rated value in $t = 22.5s$, but the steady state is reached at $t = 28s$, because there is a transient period in which the rotor speeds vary around their rated values. The mechanical and electrical torques are shown in the last two plots. As it can be observed, their responses are very similar. Even if, initially, both curves are higher than zero (0.2 pu) —motor torque—-, and they are less than zero from $t = 0.5s$, where the wind turbine produces a generator torque. The mechanical and electrical torques reach the steady state in $t = 10$ and $t = 13s$, respectively, with the rated value close to -1 pu. At $t = 20.5s$ (Fig. 12) the mechanical torques change between -0.5 and -1.5 pu in the (a), (b) and (d) curves until $t = 23s$, whereas the (c) and (e) curves the torques change to -0.5 and 0.2 pu respectively in $t = 21s$, then these torques are recovered in $t = 21.5s$ and $t = 23s$, respectively, being the steady states reached in $t = 29s$. The electrical torques have the same variations but with a negative evolution of the curves, for example the worst (e) case drops to -1.5 pu around $t = 21s$, then all electrical torques are recovered in $t = 23s$, but the steady states are reached at $t = 25s$.

VI. Conclusions

The DFIG Wind Turbine model, the three-phase fault generator along with the optimum run component have been implemented using PSCAD software. From different three-phase faults, the behaviour of the DFIG WT under these voltage sags have been simulated in PSCAD, while the results obtained were merged and plotted in MATLAB software.

The optimum run block was suitable for the PI parameter optimization during the three-phase faults, but it spent hundreds of run simulations. Moreover, other control techniques were proved in order to fulfil the requirements imposed by the REE Grid Code. The simplest form to obtain good results was the implementation of a voltage sag detector to change the references values of the active and reactive stator powers during the faults; being an equivalent option change the PI parameters of the above PI regulators during the faults, but the responses were very oscillatory. The worst solution was enabling the crowbar protection in order to avoid the higher stator currents, because in this case the RSC is temporary disable and DFIG looses the control of the rotor currents. As result the reactive power is consumption in the DFIG when the crowbar protection is activated, instead of zero or generated reactive power, which is needed at the beginning of and during the voltage fault. Definitely, the crowbar enabling is advisable in order to protect the power converter and to stop the DFIG if necessary under greater three-phase faults.

The WT responses, both electrical and mechanical values, have been compared using as reference their corresponding rated values. The global simulation results show that during the voltage dips the generator currents rise up 1.5 times in the most of cases and 2 times in the worst case, all the generator real powers drop to -0.75 pu but not all the generator reactive powers drop to 0 pu, because the worst case maintains the rated consumption of reactive power.

The WT responses (a) below unbalanced one-phase to ground voltage sag illustrate that the generator reactive power is greater than 0.4 times of the rated value, therefore the system does not fulfil all the requirements, although the generator active power is not consumed and the generator current is less than 1.5 times of the rated value. The WT behaviour (b) under unbalanced two-phase to ground voltage dip show that the generator reactive power is less than 0.4 times of the rated value, the generator active power is generated and the generator current is less than 1.5 times of the rated value, hence the system fulfils all the requirements. The WT responses (c) under balanced three-phase to ground voltage sag illustrate that the generator reactive power is less than 0.6 times of the rated value but no within 150 ms after the clearance of the fault, therefore the system does not fulfil all the requirements, moreover the generator current is almost 1.5 times of the rated value but the generator active power is not consumed. The WT behaviour (d) below unbalanced two-phase no ground voltage dip show that the generator reactive power is less than 0.4 times of the rated value, the generator active power is generated and the generator current is less than 1.5 times of the rated value, hence the system fulfils all the requirements. The WT responses (e) under balanced three-phase no ground voltage sag illustrate that the generator reactive power is less than 0.6 times of the rated value but no in the 150 ms after the clearance of the fault, moreover the generator current is greater than 2 times of the rated value but the generator active power is not consumed, therefore the system does not fulfil all the requirements.

References

[1] "Recommended practices and requirements for harmonic control in electrical power systems," IEEE Standard 519-1992.

[2] M. T. Aung and J. V. Milanovic, "The influence of transformer winding connections on the propagation of voltage sags," *IEEE Transactions on Power Delivery*, vol. 21, no. 1, pp. 262–269, January 2006.

[3] D. J. Won, S. J. Ahn, and S. I. Moon, "A modified sag characterization using voltage tolerance curve for power quality diagnosis," *IEEE Transactions on Power Delivery*, vol. 20, no. 4, pp. 2638–2643, October 2005.

[4] C. Fitzer, M. Barnes, and P. Green, "Voltage sag detection technique for a dynamic voltage restorer," *IEEE Transactions on Industry Applications*, vol. 40, no. 1, pp. 203–212, January/February 2004.

[5] I. Erlich and U. Bachmann, "Grid code requirements concerning connection and operation of wind turbines in germany," in *IEEE Power Engineering Society General Meeting*, San Francisco, California, June 2005.

[6] A. Dahlgren, C. Klippel, and A. Juntti, "Recorded fault ride through capability for two types of wind turbine generators," in *Nordic wind power conference*, Espoo, Finland, May 2006.

[7] M. F. McGranaghan, D. R. Mueller, and M. J. Samotyj, "Voltage sags in industrial systems," *IEEE Transactions on Industry Applications*, vol. 29, no. 2, pp. 391–403, 1993.

[8] M. H. J. Bollen, G. Olguin, and M. Martins, "Voltage dips at the terminals of wind power installations," *Wind Energy*, vol. 8, pp. 307–318, 2005.

[9] E. Gómez, J. A. Fuentes, A. Molina, F. Ruz, and F. Jiménez, "Results using different reactive power definitions for wind turbines submitted to voltage dips: Application to the spanish grid code," in *2006 IEEE Power Systems Conference and Expo*, October-November 2006.

[10] E. Gómez, J. Fuentes, A. Molina, F. Ruz, and F. Jiménez, "Field tests of wind turbines submitted to real voltage dips under the new spanish grid code requirements," *Wind Energy*, 2007, accepted for publication.

[11] M. H. J. Bollen, "Algorithms for characterizing measured three-phase unbalanced voltage dips," *IEEE Transactions on Power Delivery*, vol. 18, no. 3, pp. 937–944, July 2003.

[12] M. H. J. Bollen and L. D. Zhang, "Different methods for classification of three-phase unbalanced voltage dips due to faults," *Electric Power Systems Research*, vol. 66, pp. 59–69, 2003.

[13] L. Zhang and M. H. J. Bollen, "Characteristic of voltage dips (sags) in power systems," *IEEE Transactions on Power Delivery*, vol. 15, no. 2, pp. 827–832, April 2000.

[14] R. Leborgne and D. Karlsson, "Phasor based voltagge sag monitoring and characterisation," in *International Conference on Electricity Distribution*, June 2005.

[15] R. Leborgne, G. Olguin, and M. H. J. Bollen, "The influence of pq-monitor connection on voltage dip measurements," in *IEE MedPower Conference*, 2004.

[16] S. Z. Djokic, J. V. Milanovic, D. J. Chapman, and M. F. McGranaghan, "Shortfalls of existing methods for classification and presentation of voltage reduction events," *IEEE Transactions on Power Delivery*, vol. 20, no. 2, April 2005.

[17] A. Pujante, E. Gómez, and J. Fuentes, "A doubly-fed induction generator dynamic model for its use on wind power generation studies," *ICSET 2008*, 2008.

[18] E. Gómez and J. Fuentes, "Wind turbine modeling: Comparison of advanced tools for transient analysis," *PES General Meeting (IEEE PES)*, 2007.

[19] R. Pena, J. Clare, and G. Asher, "Doubly fed induction generator uising back-to-back pwm converters and its application to variable speed wind-energy generation," *This paper appears in: Electric Power Applications, IEE Proceedings*, vol. 143, pp. 231–241, 1996.